Evaluation of the Microstructure and Melting Behavior of Drawn Polypropylene Fibers with a Microthermal Analyzer

Jiping Ye,[1] T. Hasegawa,[1] A. Suzuki[2]

[1]*Research Department, NISSAN ARC, LTD, 1 Natsushima-cho, Yokosuka 237-0061, Japan*
[2]*Interdisciplinary Graduate of School of Medicine and Engineering, University of Yamanashi, Takeda-4, Kofu 400-8511, Japan*

Received 18 January 2005; accepted 21 July 2005
DOI 10.1002/app.23412
Published online in Wiley InterScience (www.interscience.wiley.com).

ABSTRACT: The strong correlation of melting behavior with the microstructure of original and zone-drawn isotactic polypropylene fibers was evaluated by microthermal analysis (micro-TA) combined with wide-angle X-ray diffraction analysis. The crystal structure of both the original and zone-drawn fibers was a monoclinic α-form with $a \sim 0.64$ nm, $b \sim 2.03$ nm, and $c \sim 0.65$ nm. In contrast to the absence of any oriented polymer molecules in the original fiber, the polymer molecules in the zone-drawn fiber were extended and highly oriented in at least two different states; one arranged along the drawn axis and the other at 40° to the drawn axis. The micro-TA-derived melting points corresponded to these microstructural changes caused by the zone-drawing process and differed from the melting points obtained by differential scanning calorimetery. The micro-TA melting point of 140°C corresponded to the z-e-p melting point of the original fiber, being much lower than the conventional differential scanning calorimetery melting point of 163°C. As for the zone-drawn fiber, an increase of 19°C in the melting temperature revealed its high orientation level, and the appearance of three elevated melting peaks (161, 167, and 178°C) at the highest heating rate (1500°C/min) coincided with its several oriented states. J Appl Polym Sci 100: 1306–1311, 2006

Key words: melting point; crystal structure; crystallization; orientation

INTRODUCTION

The melting behavior of polymers is closely related to fabrication processes such as thermal molding, thermoforming, and other thermal–mechanical processes. Different fabrication processes cause microstructural changes in crystal perfection, crystallinity, and polymer orientation. Crystal imperfections, including overly small polymer crystals and internal defects, can decrease melting enthalpy, resulting in a lower melting point.[1–4] Polymer orientation can lead to an imperfect melt in which the molecular chains are still in an orientated state,[5–6] thereby reducing melting entropy and resulting in a higher melting point. The melting behavior of polymers is thus dependent on the microstructure. Thermal analysis of melting behavior is important both for investigating the effects of various thermal and mechanical treatments used in the polymer fabrication process, and for understanding the microstructural changes that occur in the process.

Correspondence to: J. Ye (ye@nissan-arc.co.jp).

Journal of Applied Polymer Science, Vol. 100, 1306–1311 (2006)

Differential scanning calorimetery (DSC) is widely used to evaluate the melting point of polymers. However, the melting point determined by conventional DSC is independent of the polymer microstructure. The low heating rate induces crystal reorganization, which includes not only increasing the crystal size and decreasing the density of internal defects, but also recrystallizing to a crystal with a higher melting point. The DSC melting curve exhibits two melting peaks. Wunderlich and Todoki et al. demonstrated that the lower temperature peak originates from the endothermic melting of crystals and exothermic recrystallization, while the higher temperature peak arises from endothermic melting of the recrystallized materials.[1–4,7–9]

In previous studies, Todoki et al. improved the methods of preparing specimens for DSC measurement to evaluate the melting point corresponding to the polymer microstructure.[7–9] They irradiated nylon materials with γ-rays in gaseous acetylene to introduce crosslinks into the amorphous part. This specimen preparation method suppresses reorganization of imperfect crystals in the DSC heating process. The melting point thus obtained was found inherent to the original crystals and is called the zero-entropy-production (z-e-p) melting point.[2,3] They also employed

the constant–length constraint method,[8,9] in which drawn nylon fibers were bound to prevent thermal shrinkage during DSC heating. The melting point obtained was found to depend on the orientation of the molecules. These special specimen preparation methods are limited to certain polymers, and care must be taken for specimens to withstand the DSC heating process.

In recent studies, we applied an ultrahigh heating rate microthermal analysis (micro-TA) method to a zone-drawn isotactic polypropylene (it-PP) fiber.[10] This method is a convenient and powerful tool to investigate the melting behavior of the original microstructure. The micro-TA melting point decreased because of suppression of crystal reorganization or increased because of suppression of relief of the molecular orientation, as compared with the melting point obtained by traditional DSC. Because of the micro-TA probe contamination and the probe penetration into the melt at the melting point, this method is easy for obtaining the initial low temperature melting point, but difficult to detect the second or third high temperature melting peaks that originate from either various inherent states or changes in the microstructure during the measurement heating. Therefore, it is still necessary to improve this method to elucidate the instinct relationships between the melting behavior and the microstructure. This article presents the results of the study on the microstructure and melting behavior of zone-drawn it-PP fiber by combining the micro-TA method with X-ray diffraction to further investigate the strong correlation of melting properties with the detailed microstructure.

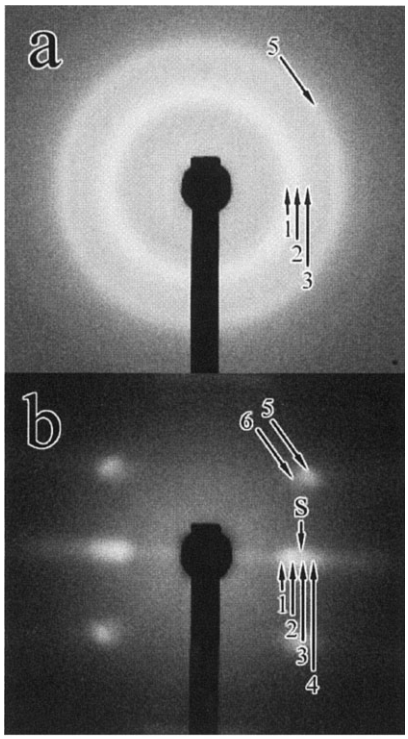

Figure 1 DSC melting curves of the original and the zone-drawn fibers measured at a heating rate of 10°C/min. The curves can be divided on the basis of two melting peaks around 153 and 163°C.

EXPERIMENTAL

A micro-TA microscope (micro-TA 2990, TA Instruments, Inc., New Castle, DE) having an ultrahigh heating rate up to 1500°C/min was used to evaluate the melting behavior of an it-PP fiber during the drawing process.[10] For reduction of influence from the micro-TA probe contamination and the probe penetration into the melt at the melting point, the sample surface was precleaned up, the probe was preannealed, and a weak scanning contact force as low as possible was used. The tip temperature was calibrated in reference to polyethylene terephthalate having a melting point of 245°C. The specimen was kept at room temperature and the spatial resolution was ~1 μm. In the DSC measurement, fibers cut to a length of 5 mm were put in an Al cell, and an empty Al cell was used as a reference. DSC was performed under nitrogen, from 30 to 200°C at a heating rate of 10°C/min. For the microstructure analysis, a wide-angle X-ray diffraction (WXRD) pattern recorded by an image plate was used to identify the crystal form and to estimate the polymer orientation.

The original fiber was melt-spun at 230°C from commercial it-PP pellets, which had a weight-average molecular weight of about 30,000 and a number-average molecular weight of about 50,000, with a tacticity of 96%. The zone-drawn fiber was prepared under a critical necking tension of 13.5 MPa at 55°C. The original fiber with a diameter of 0.60 mm was necked to the zone-drawn fiber with a diameter of 0.28 mm. Fourier transform infrared spectrometry revealed that the zone-drawn fiber possessed a higher degree of crystallinity (56%) than did the original fiber (44%). Most important, the critical necking draw ratio was 5 times that of the original fiber and the birefringence of the zone-drawn fiber was 29×10^{-3}, or nearly 6 times that (5×10^{-3}) of the original fiber.

RESULTS

Microstructure

Figure 1 shows WXRD patterns of the original and the zone-drawn fibers. The ring pattern seen in Figure 1(a) indicates that no oriented crystallites were present in

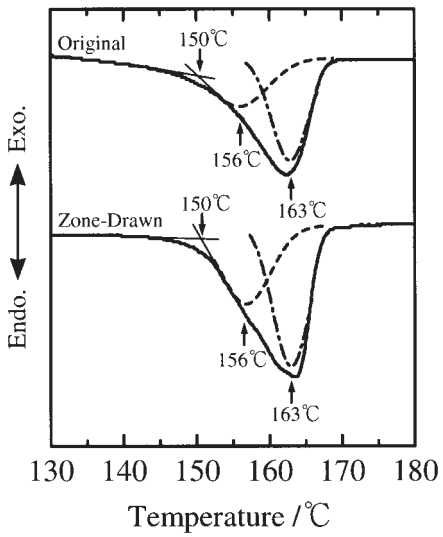

Figure 2 Wide-angle X-ray diffraction patterns of the original and the zone-drawn fibers taken along the direction perpendicular to the drawn axis.

the original fiber, and so it can be inferred that the molecules in the amorphous region were also not oriented. As shown in Figure 1(b), the ring pattern disappeared and became a spot distribution after the drawing process, indicating that the crystallites in the drawn fiber were highly oriented, with extended and oriented molecules. The broad reflections indicate that very small crystallites are present in both kinds of fibers. The strong streaks along the equatorial axis show that many face defects are present in the crystallites arranged around the drawn axis. The diffraction patterns were indexed by the monoclinic system of the α-form with $a \sim 0.64$ nm, $b \sim 2.03$ nm, and $c \sim 0.65$ nm.[11–13] Because equatorial reflections 110_α, 120_α, 040_α, and 130_α in Figure 1(b) overlapped and seemed to be an unseparated single peak, they were treated as one pseudosingle reflection. This pseudosingle reflection could be 100_s of the pseudohexagonal system of the smectic form with $a \sim 0.66$ nm and $c \sim 0.65$ nm, in which the left-hand and right-hand screw molecules have been reported to mix with each other within the unit cell.[12] Thus, the crystal structures of both the original and zone-drawn fibers are based on the α-form. The crystal structure is imperfect with a deviation from the α-form and towards the smectic form. The reflections originating from the crystallites can be separated into two groups, one oriented along the equatorial axis (the main reflections of 110_α and 120_α); the other consisted of reflection 041_α or 131_α, which strayed from the equatorial axis. The equatorial reflections thus show that the molecular chains are arranged along the drawn axis in several slightly different ways, and the 041_α and 131_α reflections indicate that the molecules are arranged at an angle of 40° to the drawn axis.

Dsc melting curves

Figure 2 shows the DSC melting curves of the original and zone-drawn fibers. No significant difference in the melting point distribution is observed between the original and zone-drawn fibers, confirming crystal reorganization and orientation relief due to DSC heating. The DSC melting curves exhibit an unsymmetrical distribution from around 150 to 163°C. The melting curves can be divided by assuming two melting peaks at 156 and 163°C with normal distributions. The melting curves show that crystallization progressed during DSC heating before 150°C. An endotherm due to melting of the crystals and an exotherm due to recrystallization occurred around 156°C; an endotherm from the melting of the recrystallized crystals took place around 163°C.

Micro-TA melting curves

Original fiber

Figure 3 shows micro-DTA and micro-TMA melting curves of the original fiber at different heating rates. Once the heated area of the fiber melted, differential power decreased due to an endothermic transition and probe displacement decreased because the probe penetrated the melt. The melting point was defined as the peak maximum in the micro-DTA melting curves. The micro-TMA melting curve was used to confirm melting behavior. At the lowest heating rate of 10°C/min, the micro-TA measurement exhibited the same melting behavior as that observed in the conventional DSC measurement, i.e., two corresponding onset points from the micro-TMA melting curve were observed at 152 and 163°C. When the micro-TA heating rate was increased to 60°C/min, the higher-tempera-

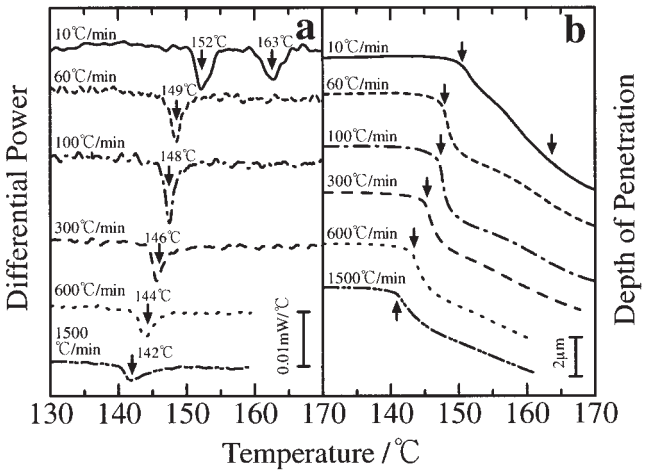

Figure 3 Micro-DTA and micro-TMA melting curves of the original fiber at different heating rates.

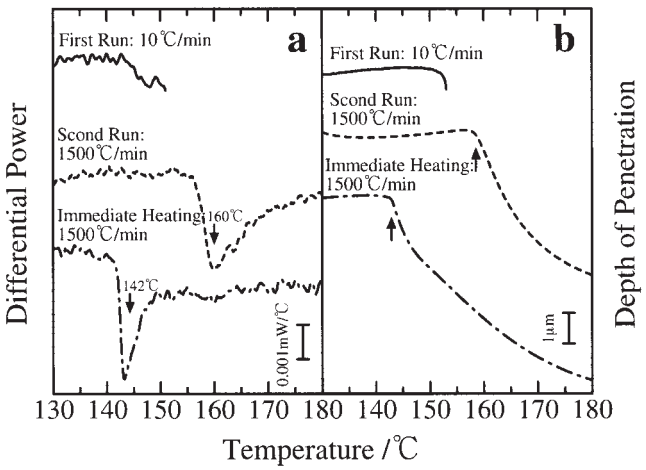

Figure 4 Micro-DTA and micro-TMA melting curves of the original fiber at a heating rate of 10°C/min in the first run and at a rate of 1500°C/min in the second run in the same local area, as well as the melting curves obtained by immediate heating at the fastest heating rate of 1500°C/min.

ture peak disappeared and the lower-temperature melting peak shifted to a lower temperature of 149°C. As the micro-TA heating rate was increased further, the lower-temperature melting peak continued to shift to lower temperatures and finally reached 142°C at the fastest heating rate. The disappearance of the higher-temperature peak shows that recrystallization was suppressed at 60°C/min.

To further investigate the suppression of crystal reorganization at a high heating rate, a second run at the fastest heating rate of 1500°C/min was applied to the same local area after the first run at the lowest rate of 10°C/min. Figure 4 shows the micro-DTA and micro-TMA melting curves obtained in the first and second runs as well as the melting curves obtained at the fastest heating rate of 1500°C/min. To reduce the influence of surface unevenness on the second-run measurement (because the probe penetrated the melt at the melting point) the specimen was heated to a temperature just below the lower-temperature melting peak at 152°C in the first run. It was found that the melting point of the second run did not decrease compared with that at 142°C under the immediate heating condition at the same fastest heating rate. The melting point of the second run was 160°C, which was very close to that of the high-temperature melting point of 163°C. The melting behavior in the second run revealed that recrystallization occurred in the first run at the low heating rate and made the melting temperature almost unrelated to the heating rate in the second run.

Zone-drawn fiber

Figure 5 shows micro-DTA and micro-TMA melting curves of the zone-drawn fiber at different heating rates. At the lowest heating rate of 10°C/min, the micro-DTA melting curve exhibited two melting peaks at 171 and 178°C and the micro-TMA melting curve displayed two corresponding onset points. As the micro-TA heating rate was increased, the higher-temperature peak disappeared at 60°C/min, and the lower-temperature melting peak continued to shift to a lower temperature of 164°C at 600°C/min. Finally, at the highest heating rate of 1500°C/min, three peaks at 161, 167, and 178°C and corresponding onset points were observed in the micro-DTA and micro-TMA melting curves. The disappearance of the higher-temperature peak and the reduction of the melting temperature were similar to the melting behavior seen for the original undrawn fiber. These melting behavior characteristics indicate that recrystallization was also suppressed in the zone-drawn fiber with a faster heating rate just as in the original undrawn fiber. Two differences in melting behavior were observed between the zone-drawn and original fibers. One was that the zone-drawn fiber possessed a higher melting temperature than the original fiber. The other was the appearance of three melting peaks at the highest heating rate of 1500°C/min. The higher melting temperature of the zone-drawn fiber suggests that the molecules remain oriented in the melt, and the three melting peaks indicate that three different orientation states exist in the melt.

To confirm that the molecules remained in the orientated state in the melt, the melting behavior of the zone-drawn fiber was observed in the first run at 10°C/min and in the second run at 1500°C/mim in the same local area. Figure 6 shows the micro-DTA and micro-TMA melting curves obtained in the first and second runs and the melting curve obtained by immediately heating the fiber at the fastest heating rate of 1500°C/min. In the first run, the maximum temperature was controlled just below the lower-temperature

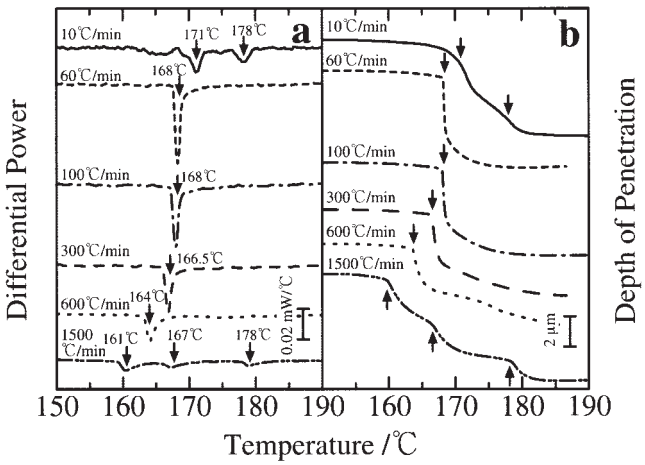

Figure 5 Micro-DTA and micro-TMA melting curves of the zone-drawn fiber at different heating rates.

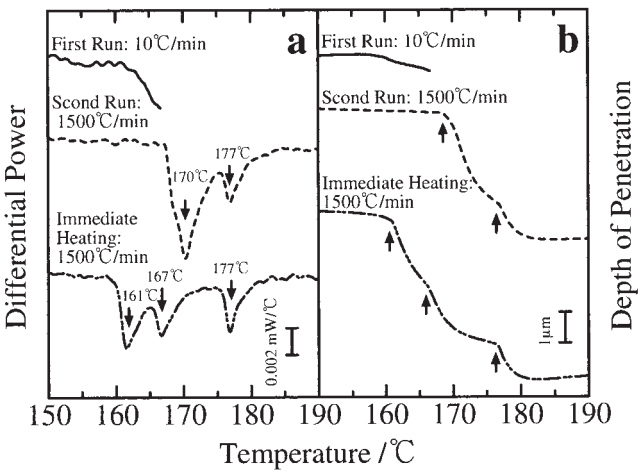

Figure 6 Micro-DTA and micro-TMA melting curves of the zone-drawn fiber at a heating rate of 10°C/min in the first run and at a rate of 1500°C/min in the second run in the same local area, as well as the melting curves obtained by immediate heating at the fastest heating rate of 1500°C/min.

peak at 171°C to reduce the influence of surface unevenness in the second run due to penetration of the probe into the melt. The melting curve in the second run had two peaks at 170 and 177°C, which were higher than the peaks at 161, 167, and 177°C in the melting curve obtained by immediate heating at 1500°C/min (Fig. 6). However, the melting peaks were close together and similar to those seen at 171 and 178°C in the melting curve obtained at the slowest heating rate of 10°C/min (Fig. 5). This observation revealed that recrystallization occurred in the first run due to the low heating rate and, consequently, the melting temperature did not increase in the second run with the higher heating rate. This observation also confirmed that the oriented molecules of the zone-drawn fiber remained in the melt even at the lowest heating rate. The melting behavior in the second run, i.e., a higher melting temperature than the conventional DSC melting point (163°C), showed that the oriented molecules were not relieved in the melt and also that the oriented state was retained after the melt solidified.

DISCUSSION

Microstructure and melting behavior

Since the WXRD analysis revealed that the molecules in the amorphous region were not oriented in the original fiber, no oriented molecules were present in the melt for elevating the melting temperature. The melting behavior of the original fiber in the micro-TA heating process was independent of the orientation factor but related to the reorganization of imperfect crystals. This presumption agrees with the micro-TA and DSC measurements. A melting temperature higher than the DSC melting point (163°C) due to the orientation factor was not observed by micro-TA. The melting temperature was found to decrease from 163 to 142°C presumably because recrystallization was suppressed by the faster micro-TA heating rate.

The WXRD analysis for the zone-drawn fiber revealed less difference in crystal perfection other than the ultrahigh orientation of the molecules as compared with the original fiber. Thus the oriented molecule chains in the amorphous region are thought to be the dominant reason for the higher melting temperature observed by micro-TA. The area around the small heated area may have restrained the molecules, causing the oriented molecules to remain in the melt. This hypothesis is verified by the results of the micro-TA analysis shown in Figure 6, where the elevation of the melting temperature due to the orientation factor was observed even in the second run.

Another melting behavior of interest for the zone-drawn fiber was the appearance of three melting peaks at the highest heating rate (1500°C/min). This suggests that several oriented states existed in the drawn fiber. The WXRD analysis confirmed that there were two types or at least two different oriented states in the amorphous region. The molecular chains were arranged along the drawn axis in several slightly different ways or arranged at an angle of 40° to the drawn axis. As shown in Figure 6, the melting curve only displayed two melting peaks, and the peak at the higher temperature disappeared at the highest heating rate (1500°C/min) in the second run. This result indicates that more highly oriented molecular chains are more easily relieved in the melt than less highly oriented ones. It is thought that the melting peak at the lowest melting temperature originated from the molecular chains arranged at an angle of 40° to the drawn axis and that the other melting peaks at higher melting temperatures originated from ones arranged along the drawn axis.

Inherent melting point and heating rate

To investigate the degree of suppression of crystal reorganization and the orientation relief of the molecule chains, the melting points (T_m) of the original and zone-drawn fibers were plotted relative to the heating rate (v_h) as shown in Figure 7. The $T_m - v_h$ plots for both fibers show that the melting temperature decreased less when the heating rate was greater than 600°C/min. Therefore, it can be assumed that the fastest heating rate of 1500°C/mm used in this micro-TA method is high enough for estimating the melting behavior inherent to the microstructure of it-PP fiber. These $T_m - v_h$ plots can be fitted aptly by $(T_m - 140) = 3600/(v_h + 300)$ for the original fiber and by $(T_m - 159) = 3600/(v_h + 300)$ for the zone-drawn fiber,

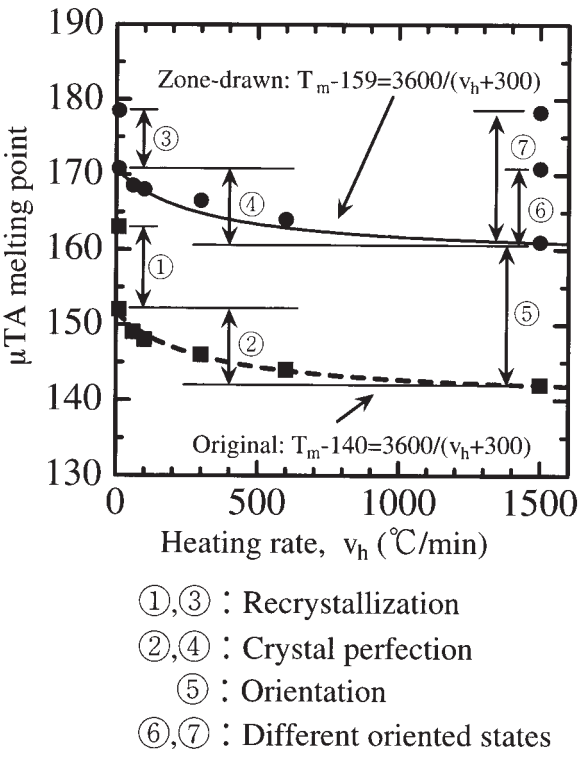

Figure 7 Dependence of the melting points on the heating rate of the original and the zone-drawn fibers.

respectively. The lower limits of T_m as v_h approaches infinity are 140°C for the original fiber and 159°C for the zone-drawn fiber, while the upper limits of T_m as v_h tends to zero are 152°C for the former fiber and 171°C for the latter one. Thus the melting point of 140°C corresponds to the z-e-p melting point of the original fiber. As shown in Figure 7, the elevation of T_m due to the inherent orientation level in the zone-drawn fiber corresponds to an increase of 19°C in T_m from the original fiber plot to the zone-drawn fiber plot. Since no significant difference in T_m is observed between v_h = 10°C/min and $v_h \to 0$, a heating rate of 10°C/min is presumed to allow complete recrystallization. The elevation of T_m due to recrystallization corresponds to an increase of 12°C from the melting temperature when $v_h \to \infty$ to that when $v_h \to 0$.

With regard to the application of this analysis method to other polymers, a micro-TA heating rate of 1500°C/min may not be high enough for estimating the melting behavior of microstructures. For nylon, a heating rate of more than 5000°C/min is needed.[7–9] Increasing the heating rate is therefore still a critical issue for the application of the micro-TA method to polymers.

References

1. Wunderlich, B. Macromolecular Physics, Vol. 3; Academic: New York, 1980.
2. Wunderlich, B. Polymer 1964, 5, 125.
3. Wunderlich, B. Polymer 1964, 5, 611.
4. Eby, R. K. J Appl Phys 1963, 34, 2442.
5. Zachmann, H. G. Kolloid Z Z Polym 1965, 25, 206.
6. Zachmann, H. G. Kolloid Z Z Polym 1969, 231, 504.
7. Todoki, M.; Kawaguchi, K. J Polym Sci Polym Phys Ed 1977, 15, 1067.
8. Todoki, M.; Kawaguchi, K. Netsu Sokutei 1985, 12, 2.
9. Todoki, M.; Kawaguchi, K. J Polym Sci Polym Phy Ed 1977, 15, 1507.
10. Ye, J.; Hasegawa, T.; Suzuki, A. J Polym Sci Part B: Polym Phys, in press.
11. Turner-Jones, A.; Aizlewood, J. M.; Beckett, D. R. Makromol Chem 1964, 75, 134.
12. Natta, G.; Corradini, P. Nuovo Cimento 1960, 15 (Suppl.), 40.
13. Bassett, D. C.; Block, S.; Piermarini, G. J. J Appl Phys 1974, 45, 4146.